

Spatial Evidence for Transition Radiation in a Solar Radio Burst

Gelu M. Nita¹, Dale E. Gary¹, and Gregory D. Fleishman^{1,2}

¹*New Jersey Institute of Technology, Newark, NJ 07102*, ²*National Radio Astronomy Observatory, Charlottesville 22903, VA, USA*

ABSTRACT

Microturbulence, i.e. enhanced fluctuations of plasma density, electric and magnetic fields, is of great interest in astrophysical plasmas, but occurs on spatial scales far too small to resolve by remote sensing, e.g., at ~ 1 -100 cm in the solar corona. This paper reports spatially resolved observations that offer strong support for the presence in solar flares of a suspected radio emission mechanism, resonant transition radiation, which is tightly coupled to the level of microturbulence and provides direct diagnostics of the existence and level of fluctuations on decimeter spatial scales. Although the level of the microturbulence derived from the radio data is not particularly high, $\langle \Delta n^2 \rangle / n^2 \sim 10^{-5}$, it is large enough to affect the charged particle diffusion and give rise to effective stochastic acceleration. This finding has exceptionally broad astrophysical implications since modern sophisticated numerical models predict generation of much stronger turbulence in relativistic objects, e.g., in gamma-ray burst sources.

Subject headings: radiation mechanisms: nonthermal – Sun: flares – Sun: radio radiation

1. Introduction

Microturbulence in cosmic sources governs the dynamics of energy release and dissipation in astrophysical and geospace plasmas, the formation of collisionless shock waves and current sheets, and is a key ingredient in stochastic acceleration (Fermi 1949; Miller et al. 1997) and enhanced diffusion (Dolginov & Toptygin 1966; Kennel & Petscheck 1966; Lee 2004) of nonthermal particles. The microturbulence may also affect the electromagnetic emission produced by fast particles, giving rise to Transition Radiation (TR), which was proposed nearly 60 years ago by two Nobel Prize winning physicists, Ginzburg and Frank (1946). TR in its original form (Ginzburg and Frank 1946) results from a variation in phase speed of wave propagation at transition boundaries. The theory of TR has seen wide application in the laboratory (Cherry et al. 1974) and in cosmic ray detectors (Favuzzi et al.

2001; Wakely et al. 2004), although no naturally occurring radiation had been confirmed as TR.

In the astrophysical context, TR must arise whenever nonthermal charged particles pass near or through small-scale inhomogeneities such as wave turbulence or dust grains. However, it was thought to be weak, and perhaps unobservable (Durand 1973; Yodh, Artru & Ramaty 1973; Fleishman & Kahler 1992), until Platonov & Fleishman (1994) showed that its intensity can be greatly enhanced due to plasma resonance at frequencies just above the local plasma frequency. Spatially and spectrally resolved observations of this resonant transition radiation (RTR), if present, can provide quantitative diagnostics of plasma density, and of the level of microturbulence in the flaring region.

A number of recent publications, based mainly on studies of individual events, indicate that RTR may be produced in solar radio bursts (Fleishman 2001; Fleishman, Melnikov, & Shibasaki 2002; Lee et al. 2003; LaBelle et al. 2003; Bogod & Yasnov 2005). Most recently, we have described the observational characteristics expected for RTR in the case of solar bursts (Fleishman, Nita, & Gary 2005), and found that the correlations and associations predicted for total power data are indeed present in the decimetric ($\sim 1\text{-}3$ GHz) components of a statistical sample of two-component solar continuum radio bursts. However, interpretations based on non-imaging data remain indirect (and, thus, ambiguous) until they can be combined with direct imaging evidence from multi-wavelength spatially resolved observations, which were missing in the previous studies.

This report presents comprehensive (radio, optical, and soft X-ray) spatially resolved observations for one of the RTR-candidate bursts. As we describe below, these observations provide primarily three new confirmations: (1) the RTR and gyroemission sources are co-spatial, (2) the RTR component is associated with a region of high density, and (3) the RTR emission is o -mode polarized. Together with the already demanding spectral and polarization correlations found previously (Fleishman, Nita, & Gary 2005), these new observations provide further strong evidence in favor of RTR.

2. Theoretical Expectations

The two spectral components of such RTR candidate bursts (one at centimeter wavelengths due to the usual gyrosynchrotron (GS) mechanism, and one at decimeter wavelengths suspected as RTR), must be *co-spatial* to allow an unambiguous RTR interpretation. An alternative explanation of such two-component bursts is that both spectral components are produced by the same (GS) emission mechanism (with different parameter combinations in

the two components), but if the low and high frequencies come from the same source location this should merely broaden the spectrum. Having truly separate spectral components requires either completely different source locations, or different mechanisms, or both. Distinct spectral components having the *same source location* is a strong indicator that each component is produced by *a different emission mechanism*. Therefore, direct observation of the spatial relationship between the spectral components of RTR candidate bursts is the key evidence needed to conclude the emission mechanism producing the decimetric spectral component.

The theory of RTR in the astrophysical context is discussed in detail in a recent review paper (Platonov & Fleishman 2002). RTR arises as fast particles move through a plasma with small-scale variations (as short as the wavelength of the emitted wave) of the refractive index. Such variations may be provided by microturbulence-induced inhomogeneities of the plasma density or magnetic field.

In the case of solar bursts, the main properties of this emission mechanism that can be checked against observations are: (1) originates in a dense plasma, $f_{pe} \gg f_{Be}$, where f_{pe} and f_{Be} are the electron plasma- and gyro-frequencies; (2) has a relatively low peak frequency in the decimetric range, and so appears as a low-frequency component relative to the associated GS spectrum; (3) is co-spatial with or adjacent to the associated GS source; (4) varies with a time scale comparable to the accompanying GS emission (assuming a constant or slowly varying level of the necessary microturbulence); (5) is typically strongly polarized in the ordinary mode (*o*-mode), since the extraordinary mode (*x*-mode) is evanescent, as for any radiation produced at the plasma frequency in a magnetized plasma; (6) is produced typically by the lower-energy end of the same nonthermal electron distribution that produces the GS emission, with the *emissivity proportional to the instantaneous total number* of the low-energy electrons in the source *at all times during the burst* (in contrast to plasma emission, whose highly nonlinear emissivity is largely decoupled from electron number even though it may for a time display a similar proportionality); (7) has a high-frequency spectral slope that does not correlate with the spectral index of fast electrons (in contrast to GS radiation, which does).

3. Data Analysis

Figure 1 presents the dynamic spectrum of the 2001 April 06 solar radio burst in intensity and circular polarization, observed with the Owens Valley Solar Array (Gary & Hurford 1999) (OVSA). This event is one of many observed with OVSA whose spectral behavior matches the expectations for RTR (Fleishman, Nita, & Gary 2005), but is the first for which

detailed spatial comparison has been made. The RTR occurs at a restricted range of time and frequency shown by the bright red region in the bottom panel, which represents highly right hand circularly polarized (RCP) emission. The results presented in Figures 2 and 3 confirm the expected spatial association of the RTR radio source with (i) the accompanying GS source, (ii) an unusually dense soft X-ray loop, and (iii) the underlying magnetic field structure, and hence offer further support for its interpretation as RTR emission. Comparing the required observational characteristics in the order 1–7 presented above, we find:

1. Both the RTR (2 GHz) and GS (7.4 GHz) sources arise in or near an unusually dense loop. The electron temperature inferred from SXT data (Fig. 3), averaged over the pixels lying inside the 85% 2 GHz RCP contour, is 2×10^7 K, while the average emission measure corresponding to one pixel (2.5×2.5 arcsec) is 5.6×10^{48} cm⁻³. Assuming a line of sight length of ~ 25 arcsec, the projected loop width, we obtain an estimate for the plasma density in the region as 3×10^{11} cm⁻³. This value directly confirms the existence of a high plasma density in the flaring region, as suggested by the Razin effect diagnosis we employed previously (Fleishman, Nita, & Gary 2005). The RTR peak frequency of 2 GHz implies, from the electron plasma frequency $f_{pe} = 9 \times 10^3 \sqrt{n}$ Hz, an electron density of 5×10^{10} cm⁻³, compared with 3×10^{11} cm⁻³ derived above for the underlying soft X-ray loop. The X-ray-derived density demonstrates the presence of high densities in the region, while the lower radio-derived density is expected since the 2 GHz radio emission will come primarily from overlying, less-dense regions due to significant free-free absorption in the higher-density regions.
2. As seen in Fig. 1, the RTR forms a distinct, low-frequency spectral component relative to the higher-frequency GS component.
3. Figs. 2 and 3 show that the RTR and GS sources are co-spatial. As already emphasized, this co-spatiality is highly conclusive in favor of RTR, since separate spectral components (of multi-component bursts) typically come from distinct locations (Gary & Hurford 1990; Benz, Saint-Hilaire, & Vilmer 2002).
4. Both spectral components are smooth in time and frequency, with comparable time scales, the main difference being that the GS component is delayed with respect to the RTR component (see Figs. 1 and 4). Note also in Fig. 4 the similarity of high-energy HXR with the GS (7.4 GHz) component, and low-energy HXR with the RTR (2 GHz) component, which we discuss in more detail in item 6, below.
5. Figs. 1 and 2 show that the RTR emission is strongly polarized in the sense of the *o*-mode, as required, while the GS emission is *x*-mode. The radio maps at 7.4 GHz in Fig. 2 (filled contours) reveal RCP (red) overlying positive (white) magnetic polarity

and LCP (blue) overlying negative (black) polarity, located on opposite sides of the neutral line. This clearly shows a relatively high degree of x -mode polarization of both 7.4 GHz radio sources. At 2 GHz (unfilled contours), exactly the opposite spatial correspondence is seen, with RCP (red) overlying negative magnetic polarity and (the much weaker) LCP (blue) slightly shifted toward positive polarity. This clearly shows a high degree of o -mode polarization for the RTR spectral component.

6. Indirect statistical evidence for the RTR component being due to low energy electrons was obtained from spectral correlations (Fleishman, Nita, & Gary 2005).¹ A more reliable estimate of the energy of the fast electrons involved comes from a comparison of the radio and hard X-ray light-curves in Figure 4. We first note the similarity of the RTR light curve and the 41-47 keV hard X-ray light curve. As shown by Nitta & Kosugi (1986), hard X-rays are due to electrons of energy 2-3 times higher than the photon energy, so that 41-47 keV HXR correspond to $\sim 100 - 150$ keV electrons. In contrast, the GS light curve at 7.4 GHz displays a poor correlation with 41-47 keV HXR, but an excellent correlation with the higher energy HXR light curve, at 128-157 keV, produced by the electrons of $\sim 250 - 450$ keV. This is consistent with the well known result that GS emission comes from electrons of energy typically > 300 keV (Bastian, Benz, & Gary 1998). The similarity of the shape and timing of the 128-157 keV HXR and 7.4 GHz light curves, and those of the 41-47 keV HXR and 2 GHz light curves, is consistent with their being due to electrons of energies $\gtrsim 300$ keV and $\lesssim 150$ keV, respectively. It is reasonable to conclude that the RTR and GS emission, being essentially co-spatial, are from different parts of a single electron energy distribution.
7. As reported in an earlier paper (Fleishman, Nita, & Gary 2005, fig.7) the high-frequency slopes of the RTR and GS spectra for this event are uncorrelated, which provides an independent confirmation that the low-frequency component is not simply a low-frequency GS source.

¹Note that in most incoherent emission mechanisms, the spatially resolved brightness temperature provides a lower limit to the energy of emitting electrons. The brightness temperature of the 2 GHz RCP source in Fig. 2 reaches 2.5×10^9 K, which for the typical incoherent mechanism would correspond to a particle energy of about 220 keV (indeed lower than the energy of the synchrotron emitting fast electrons specified below). However, for the RTR case this argument is inconclusive since the brightness temperature of RTR depends on effective energies of both fast electrons and nonthermal density fluctuations, rather than of fast electrons only.

4. Discussion

The above characteristics rule out standard GS emission for the low-frequency spectral component, while they are expected and agree fully with RTR. An alternative model that might account for the presence of a co-spatial, yet distinct dm-continuum spectral component—quasi-stationary plasma emission due to a marginally stable regime of a loss-cone instability—is much more difficult to eliminate, or even distinguish from RTR. Indeed, properties 1, 2, 6, 7 are typical also for plasma emission, and properties 3, 4, 5, while not required for plasma emission, are not inconsistent with it. We believe that the key evidence distinguishing RTR from plasma emission is the strict proportionality between the radio flux and the number of emitting electrons on all time scales, as suggested by the agreement between the RTR time profile and the low-energy hard X-ray light curve of Fig. 4. This proportionality, based on the spectral properties of the dm bursts, was found in all of the bursts studied by Fleishman, Nita, & Gary (2005). We note, however, that a temporal resolution better than the 4 s we have available will be needed to check this property down to millisecond time scales.

Nevertheless, we looked for further evidence favoring the plasma emission interpretation of the smooth dm component and conclude that this model (even though not firmly eliminated) is not supported by the data. For example, the high degree of o -mode polarization of the dm continuum implies fundamental rather than harmonic plasma emission, although the latter is typically much easier to generate in the coronal plasma. However, spectra in this burst and in the other bursts studied by Fleishman, Nita, & Gary (2005), at no time show any hint of a second harmonic spectral feature. Furthermore, quasi-steady plasma emission requires a significant loss-cone anisotropy, which in turn gives rise to a widely observed loop-top peak brightness for the optically thin GS radio emission (Melnikov et al. 2002). In contrast, the 7.4 GHz source displays a clear separation into x -polarized kernels (corresponding to leg or foot-point sources, rather than a loop-top source), thus, any pitch-angle anisotropy is at best very modest. This conclusion is also supported by the statistical evidence found in (Fleishman, Nita, & Gary 2005) in favor of more isotropic (than on average) distributions of the fast electrons in the RTR-producing bursts. Therefore, all the properties specific for RTR and those common for both RTR and plasma emission are observed, while no specific property expected solely for the plasma emission is seen, which leads us to favor RTR.

We have presented ample evidence that the decimetric component of the 2001 April 06 radio burst near 19:23 UT is produced by the RTR mechanism. Since this event is one among a set of other events with similar, unique characteristics, the evidence presented here supports the conclusions made by Fleishman, Nita, & Gary (2005), based on total power

data for a statistical sample of the bursts candidates, that these bursts are due to RTR.

The importance of this result is several-fold. First, it strengthens the case for RTR as another incoherent continuum emission mechanism in astrophysical plasmas, among only a small number of others: gyrosynchrotron/synchrotron emission, bremsstrahlung, and inverse Compton emission. Second, there are a few types of solar radio continuum, e.g., type I and type IV m/dm, which are conventionally ascribed to plasma emission. We point out that this interpretation has never been quantitatively proved, and RTR represents a plausible alternative to the current interpretation, which we believe calls for revisiting the issue of the origin of non-GS solar radio continua. Third, with new radio facilities in development that are capable of simultaneous spatial and spectral measurements of solar bursts (e.g. Expanded VLA (Perley et al. 2004) and Frequency Agile Solar Radiotelescope (FASR) (Bastian 2004)), RTR can be routinely recognized and used as a diagnostic of the plasma density, the low-energy part of the electron energy distribution, and of the presence and quantitative level of microturbulence. In this event, for example, the level of inhomogeneities derived from the RTR flux, described by Eq. (403) in Platonov & Fleishman (2002), is $\langle \Delta n^2 \rangle / n^2 \sim 10^{-5}$. Thus, RTR may provide a sensitive tool for measuring this elusive but important quantity.

We acknowledge NSF grant AST-0307670 and NASA grant NAG5-11875 to NJIT. The NRAO is a facility of the NSF operated under cooperative agreement by Associated Universities, Inc. We gratefully acknowledge the help of J. Qiu in providing the X-ray and MDI data.

REFERENCES

- Acton, L., Tsuneta, S., Ogawara, Y., Bentley, R., Bruner, M., Canfield, R., Culhane, L., Doschek, G., Hiei, E. & Hirayama, T. 1992, *Science*, 258(5082), 618
- Bastian, T.S., Benz, A.O. & Gary, D.E. 1998, *ARA&A*, 36, 131
- Bastian, T.S. 2004, in *Solar and Space Weather Radiophysics*, (Eds – D. E. Gary & C. U. Keller, *Astrophysics and Space Science Library*, Kluwer), 314, 47
- Benz, A. O., Saint-Hilaire, P., Vilmer, N. 2002, *A&A*, 383, 678
- Bogod, V.M., & Yasnov, L.V. 2005, *Astron. Repts.*, 49, 144
- Cherry, M.L., Hartmann, G., Muller, D. & Prince, T.A. 1974, *Phys. Rev. D*, 10(11), 3594
- Dolginov, A.Z., & Toptygin, I.N. 1966, *ZhETF*, 51, 1771
- Domingo, V., Fleck, B. & Poland, A. I. 1995, *Sol. Phys.*, 162, 1
- Durand, L. 1973, *ApJ*, 182, 417
- Favuzzi, C., Giglietto, N., Mazziotta, M.N. & Spinelli, P. 2001, *Riv. Nuovo Cim.* 24(5-6), 1
- Fermi, E., *Phys. Rev.* 1949, 75(8), 1169
- Fleishman, G.D. 2001, *Astronomy Letters*, 26, 254
- Fleishman G.D. & Kahler S.W. 1992, *ApJ*, 394, 688
- Fleishman, G.D., Nita, G.M. & Gary, D.E. 2005, *ApJ*, 620, 506
- Fleishman, G.D., Melnikov, V.F., & Shibasaki, K., *Proc. 10th European Meeting on Solar Physics*, Prague, Czech Rep., 9-14 September 2002
- Gary, D. E. & Hurford, G. J. 1990, *ApJ*, 361, 290
- Gary, D.E. & Hurford, G.J. 1999, in *Proceedings of the Nobeyama Symposium, Kiyosoto, Japan*, NRO Rep. 479, 429
- Ginzburg, V.L. & Frank, I.M. 1946, *Zh. Eksp. Teor. Fiz.* 16, 15
- Kennel, C. F. & Petscheck, H. E. 1966, *J. Geophys. Res.*, 71, 1
- LaBelle, J., Treumann, R. A., Yoon, P. H., & Karlicky, M. 2003, *ApJ*, 593, 1195

- Lee, J.W. 2004, in *Solar and Space Weather Radiophysics*(Eds - D. E. Gary & C. U. Keller, Astrophysics and Space Science Library, Kluwer), 314, 179
- Lee, J., Gallagher, P.T., Gary, D.E., Nita, G.M., Choe, G.S., Bong, S.C. & Yun, H.S. 2003, *ApJ*, 585, 524
- Melnikov, V.F., Shibasaki, K., & Reznikova, V.E. 2002, *ApJ*, 580, L185
- Miller, J. A., Cargill, P. J., Emslie, A., Holman, G. D., Dennis, B. R., Larosa, T. N., Winglee, R. M., Benka, S. G. & Tsuneta, S. 1997, *J. Geophys. Res.*, 102, 14631
- Nitta, N. & Kosugi, T. 1986, *Sol. Phys.*, 105, 73
- Platonov K.Yu. & Fleishman G.D. 1994, *Zh. Exper. Teor. Fiz.*, 106(4), 1053 (transl.: *JETP*, 79(4), 572-580).
- Platonov K.Yu. & Fleishman G.D. 2002, *Uspekhi Fiz. Nauk.*, 172(3), 241(transl.: *Physics Uspekhi*, 45(3), 235-291).
- Perley, Richard A., Napier, Peter J. & Butler, Bryan J. 2004, *Proceedings of the SPIE*, 5489, 484
- Qiu, J. & Gary, D. E. 2003, *ApJ*, 599(1), 615
- Wakely, S. P. , Plewnia, S., Muller, V., Horandel, J. R. & Gahbauer, F. 2004, *Nuclear Instruments and Methods in Physics Research Section A*, 531(3), 435
- Yodh, G. B., Artru, X., & Ramaty, R. 1973, *ApJ*, 181, 725

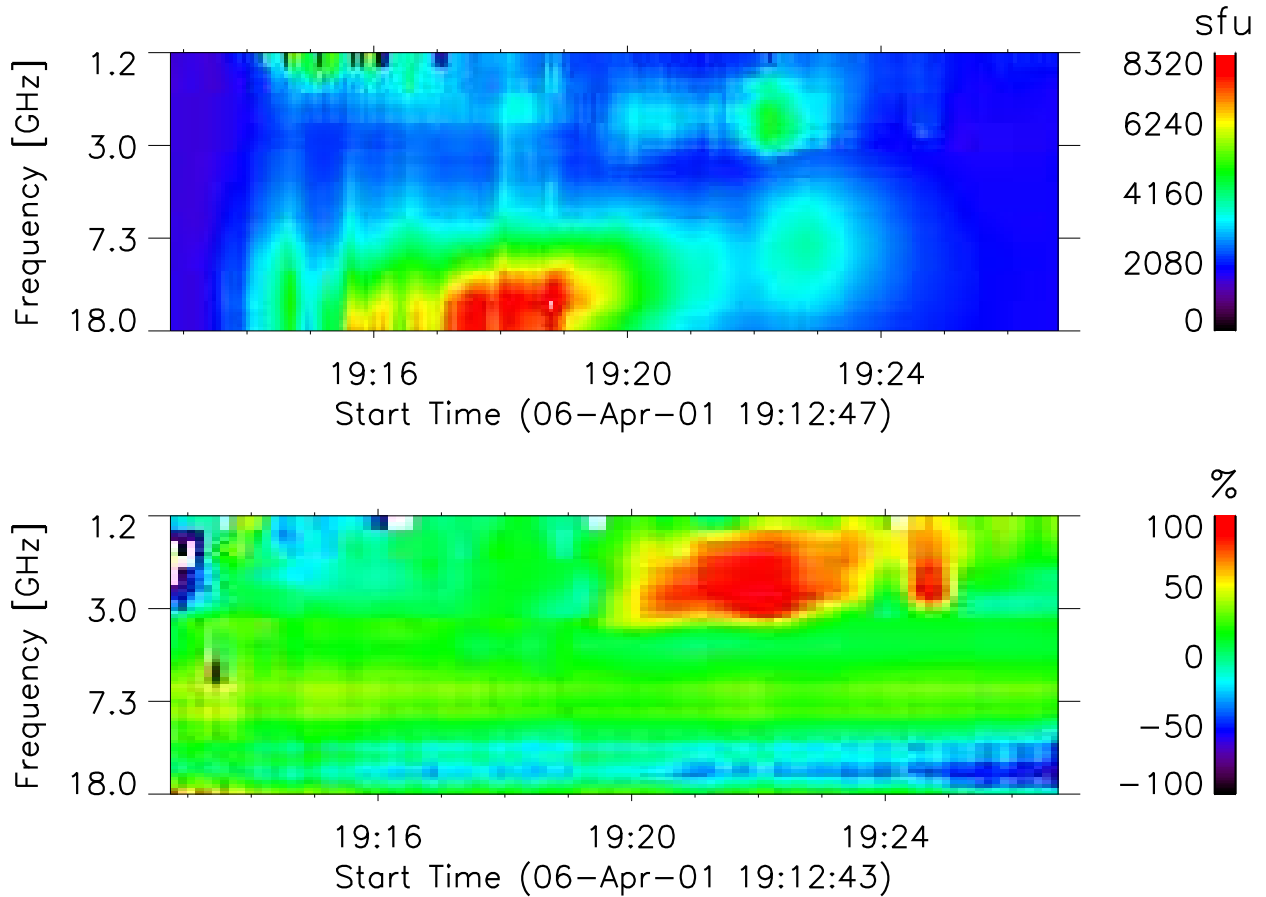


Fig. 1.— 2001 April 06 after 19:12 UT. Upper panel: Total power dynamic spectrum recorded by OVSA with 4 s time resolution at 40 frequencies in the [1.2–18] GHz range. Lower panel: Dynamic spectrum of circular polarization with 8 s time resolution at the same frequencies as in the upper panel. The period of RTR is the highly polarized (red) emission in the lower panel. Two spectral components are visible in the upper panel during this time: the low frequency RTR component, which peaks at 19:22:11 UT (3700 sfu at 2 GHz), and the delayed high frequency GS component, which peaks at 19:22:51 UT (2300 sfu at 7.4 GHz).

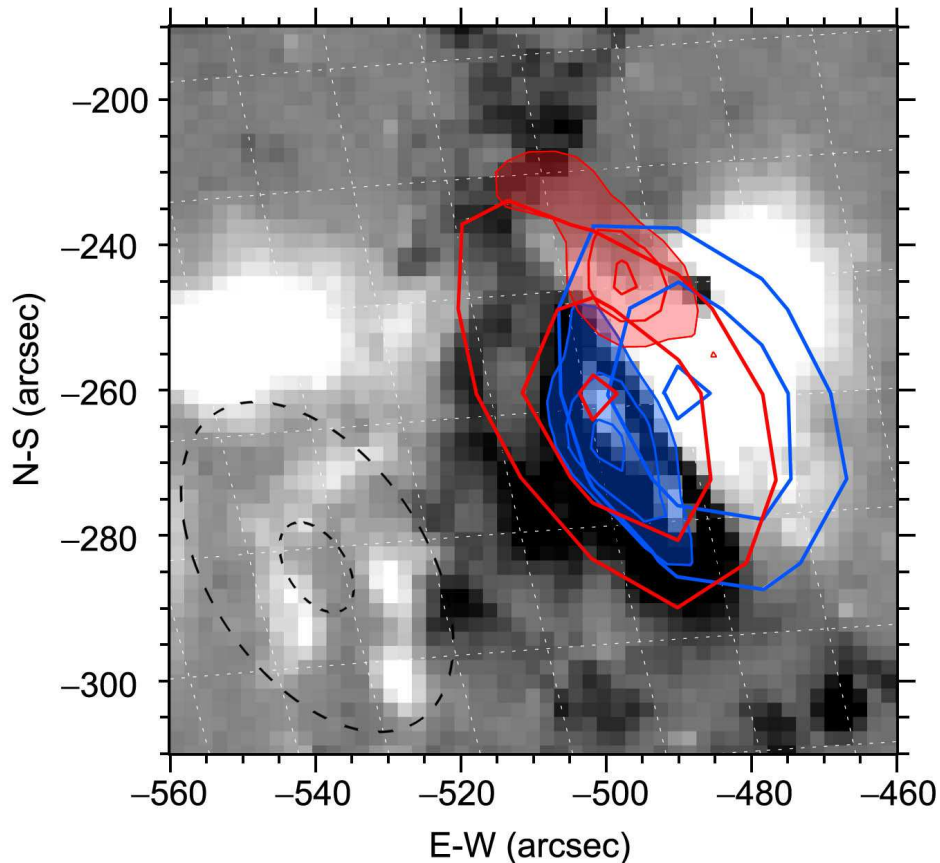


Fig. 2.— 2001 April 06, OVSA radio maps (19:22:03 UT). The RCP (red contours) and LCP (blue contours) at 2 GHz (unfilled contours) and 7.4 GHz (filled contours) are overlaid on the SOHO (Domingo, Fleck, & Poland 1995) MDI magnetogram (19:22:02 UT). The dashed ovals represent the half power OVSA beam at the two selected frequencies. The radio contours are scaled separately for each frequency and polarization, and only 3 are shown for clarity, representing 55, 75, and 95% of the maximum intensity. The maximum brightness temperatures are 2500 MK (2 GHz RCP), 770 MK (2 GHz LCP), 880 MK (7.4 GHz RCP) and 600 MK (7.4 GHz LCP). Small islands of apparent magnetic field sign reversal in regions of both polarities are an instrumental artifact (Qiu & Gary 2003) and not real. Within the instrumental resolution (see the corresponding beam size), the 2 GHz RCP source (red, unfilled contour) is co-located with the 7.4 GHz LCP source (blue, filled contour) in the negative magnetic field region. We conclude that both low and high frequency emissions are likely produced by the same population of electrons travelling along the same magnetic loop. Remarkably, for both frequencies, the *intrinsic* degrees of polarization implied by the radio maps are noticeably larger than those suggested by the unresolved polarization spectrum presented in the lower panel of Fig. 1.

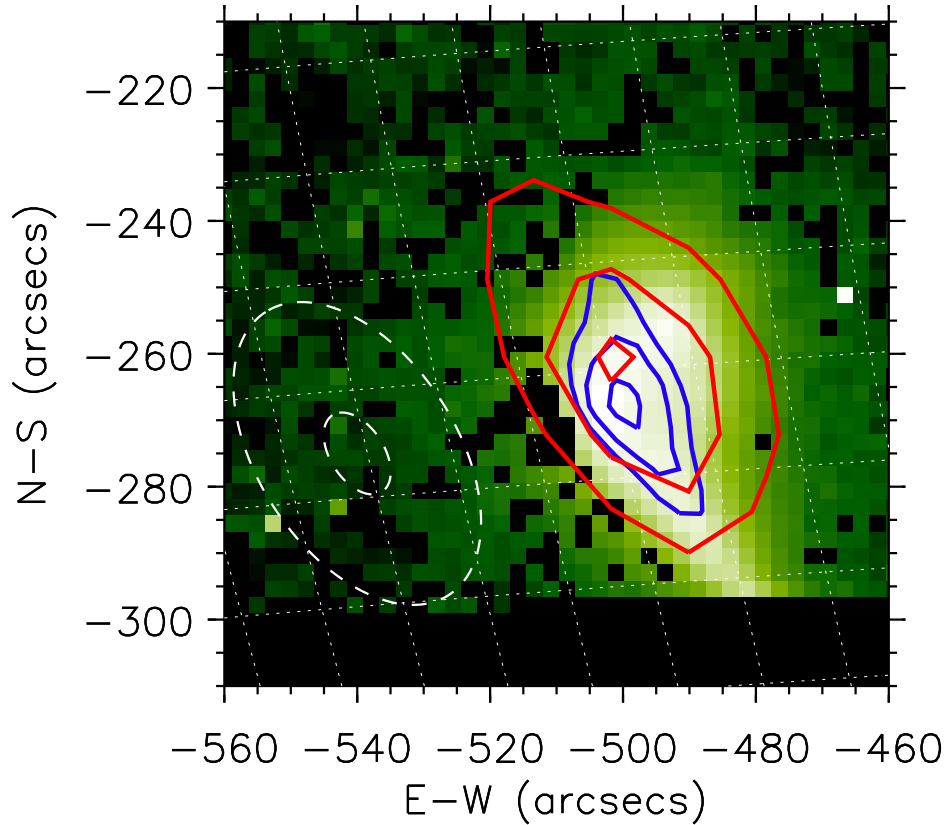


Fig. 3.— 2001 April 06. Emission measure (EM) map (19:22:00 UT) derived from the Yohkoh SXT instrument (Acton et al. 1992), using data obtained with two different filters (Be119 and Al12). For clarity, only the OVSA (19:22:03 UT) RCP 2 GHz (red contours) and LCP 7.4 GHz (blue contours) are overlaid here. The EM map reveals the existence of a magnetic loop or arcade of loops filled with hot and dense plasma, which is consistent with the magnetic and radio topology presented in Fig. 2. The 2 GHz RCP radio source and the 7.4 GHz LCP kernel are well aligned with the most dense section of the loop.

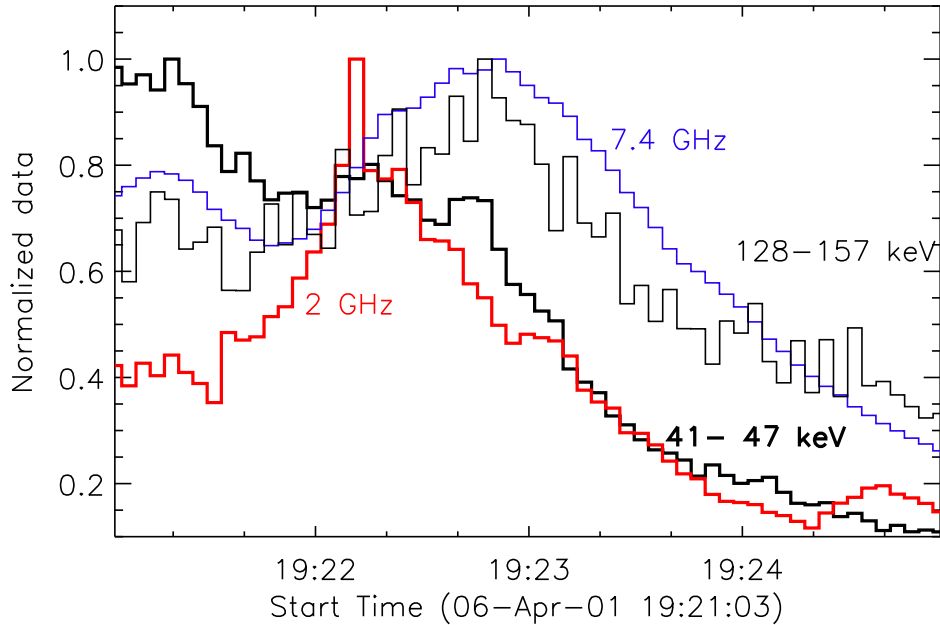


Fig. 4.— OVSA total power lightcurves at 2 GHz (red line) and 7.4 GHz (blue line), and Yohkoh (Acton et al. 1992) WBS hard X-ray counts in the 41-47 keV (thick line) and 128-157 keV (thin line) ranges. Each curve has been normalized to the corresponding maximum values recorded after 19:21 UT (3700 sfu at 2 GHz, 2300 sfu at 7.4 GHz, 2088, and 244 HXR counts, respectively). The 128-157 keV hard X-ray and 7.4 GHz time profiles are similar, which is consistent with the 7.4 GHz emission being due to electrons of energy > 300 keV. The RTR emission at 2 GHz peaks about 1 min earlier, has quite different time behavior, and best correlates with the 41-47 keV hard X-rays channel, reflecting the fact that it is due to a lower-energy part of the same population, and also depends on other parameters such as the level of density fluctuations.